

Narrow-bandwidth high-order harmonics driven by long-duration hot spots

This content has been downloaded from IOPscience. Please scroll down to see the full text.

2012 New J. Phys. 14 063036

(<http://iopscience.iop.org/1367-2630/14/6/063036>)

View [the table of contents for this issue](#), or go to the [journal homepage](#) for more

Download details:

IP Address: 141.213.172.165

This content was downloaded on 24/10/2013 at 07:03

Please note that [terms and conditions apply](#).

Narrow-bandwidth high-order harmonics driven by long-duration hot spots

Maxim Kozlov^{1,6}, Ofer Kfir¹, Avner Fleischer¹, Alex Kaplan^{1,2},
Tal Carmon², Harald G L Schwefel^{3,4}, Guy Bartal⁵
and Oren Cohen¹

¹ Solid State Institute and Physics Department, Technion, Haifa 32000, Israel

² Electrical Engineering and Computer Science, University of Michigan,
Ann Arbor, MI 48109, USA

³ Institute for Optics, Information and Photonics, University of
Erlangen-Nuremberg, Erlangen D-91058, Germany

⁴ Max-Planck-Institute for the Science of Light, Erlangen D-91058, Germany

⁵ Electrical Engineering Department, Technion, Haifa, 32000, Israel

E-mail: kozlov@si-sun1.technion.ac.il

New Journal of Physics **14** (2012) 063036 (14pp)

Received 23 January 2012

Published 26 June 2012

Online at <http://www.njp.org/>

doi:10.1088/1367-2630/14/6/063036

Abstract. We predict and investigate the emission of high-order harmonics by atoms that cross intense laser hot spots that last for a nanosecond or longer. An atom that moves through a nanometer-scale hot spot at characteristic thermal velocity can emit high-order harmonics in a similar fashion to an atom that is irradiated by a short-duration (picosecond-scale) laser pulse. We analyze the collective emission from a thermal gas and from a jet of atoms. In both cases, the line shape of a high-order harmonic exhibits a narrow spike with spectral width that is determined by the bandwidth of the driving laser. Finally, we discuss a scheme for producing long-duration laser hot spots with intensity in the range of the intensity threshold for high-harmonic generation. In the proposed scheme, the hot spot is produced by a long laser pulse that is consecutively coupled to a high-quality micro-resonator and a metallic nano-antenna. This system may be used for generating ultra-narrow bandwidth extreme-ultraviolet radiation through frequency up-conversion of a low-cost compact pump laser.

⁶ Author to whom any correspondence should be addressed.

Contents

1. Introduction	2
2. Model	3
3. Single-atom spectra	5
4. Multiple atoms spectra	8
5. Generation of high-intensity long-duration hot spots	12
6. Conclusions	13
Acknowledgments	13
References	13

1. Introduction

Extreme-ultraviolet (EUV) light of high spatial and temporal coherence is in high demand for a wide range of applications such as spectroscopy, precision measurements, coherent imaging, holography, etc. [1]. Such light can be produced through the highly nonlinear process of high-harmonic generation (HHG). High-order harmonics are produced by focusing a very intense driving laser into nonlinear media, typically a noble gas. When an atom is irradiated by an intense laser pulse, whose peak electric field is close in magnitude to the Coulomb field of the atom, the outermost electron may be ionized from the atom. The released electron is accelerated by the electric field of the light, first moving away from the ion, then as the field changes direction, back toward it. The electron may then recombine with the ion, releasing its excess energy in the form of a highly energetic photon. The high harmonics spectra exhibit a plateau region, whereby the intensity of the harmonics remains approximately constant over many harmonic orders [2, 3]. The threshold intensity for tunneling ionization and HHG from atoms (e.g. xenon) and molecules (e.g. benzene) is in the range of $10^{13} \text{ W cm}^{-2}$ [4] (at lower intensity, higher harmonics are produced through perturbative nonlinear processes and their intensity exhibits exponential decay with harmonic order). The intensity threshold for HHG is, to-date, obtained by concentrating the laser energy into pulses with picosecond to femtosecond pulse duration [5, 6]. Importantly, the fact that the process is driven by short laser pulses prevents the depletion of the bound state by the leading edge of the laser pulse through multi-photon ionization [7]. To-date, intense short laser pulses for driving HHG are typically obtained by amplification of short pulses that are first produced by an oscillator. This scheme includes a significant reduction in the laser repetition rate, typically from $\sim 100 \text{ MHz}$ at the oscillator output to $\sim 1 \text{ kHz}$. The use of novel fiber amplifiers allowed HHG with $\sim 1 \text{ MHz}$ repetition rate [8]. Two approaches have been demonstrated for achieving the intensity threshold for HHG directly from $\sim 100 \text{ MHz}$ repetition rate oscillators. In the first approach, the femtosecond laser pulses are coupled to an external cavity that contains the nonlinear medium (noble gas) [4, 9, 10]. The finesse of these cavities is limited to ~ 1000 because the bandwidth of the cavity must support the femtosecond pulses that circulate inside. In the second approach, intensity is enhanced through sub-wavelength focusing by surface plasmons [11, 12]. Specifically, HHG was demonstrated using an array of gold bow-tie nano-antennas [13, 14] and metallic waveguide [15]. In both approaches, the high repetition rate of the driving laser may result in HHG with high temporal coherence.

Nevertheless, the total spectral bandwidth of each harmonic is relatively broad because it is limited by the spectral bandwidth of the driving laser, which in turn is limited by the inverse of its pulse duration.

Here, we investigate emission of high-order harmonics from atoms that move through intense laser hot spots that last for a nanosecond or longer. An atom that moves through a hot spot experiences a field of varying intensity in a similar fashion to a stationary atom that is irradiated by a short-duration laser pulse. If the size of the hot spot is in the nanometer scale and the velocity of the atom is several hundreds of meters per second (thermal velocity at 300 K) then the duration of crossing through the hot spot (cross-duration) is in the picosecond timescale, which is short enough to avoid bound-state depletion [6]. Thus, the atoms crossing the hot spot can emit pulses of high-order harmonics. The duration of the pulse emitted by an individual atom is proportional to the cross-duration. Hence, the bandwidth of such pulses is inversely proportional to the cross-duration. In the case of a thermal gas, the trajectories of the atoms are stochastic. As a result, the emission resembles a sequence of varying pulses that are randomly distributed in time. Our analysis shows that these pulses are all phase locked with the driving laser field and are hence highly correlated. This results in a power spectrum that is dominated by a narrow spike. The width of the spike is determined by the bandwidth of the driving laser and is independent of the average cross-duration. Therefore, the emitted EUV radiation can have ultra-narrow bandwidth if it is driven by a long-duration highly coherent laser. Finally, we discuss a possible scheme for producing long-duration, highly coherent, intense, laser sub-wavelength hot spots. In the proposed scheme, the hot spot is produced by a long laser pulse that is consecutively coupled to a high-quality micro-resonator [16–21] and a metallic nano-antenna. This scheme may be used for generating ultra-narrow bandwidth EUV radiation through frequency up-conversion of a low-cost compact pump laser.

The paper is organized as follows. The model is presented in section 2. The properties of emission by a single atom that crosses the hot spot are presented in section 3. The collective emission by multiple atoms is analyzed in section 4. Finally, section 5 discusses the proposed scheme for generation of high-intensity long-duration hot spots.

2. Model

Emission of high-order harmonics from atoms in intense laser hot spots was demonstrated experimentally [13] and recently investigated theoretically [22]. Similar to the previous studies [22–24], we assume that the electric field in the sub-wavelength hot spot is linearly polarized (in general, the polarization of electric field depends on the shape of the nano-antenna used to generate the hot spot). The standard dipole approximation, which assumes a homogeneous electric field, is unsuitable for HHG from hot spots because the characteristic length scale of the electron orbit becomes comparable to the length-scale over which the intensity changes. Thus, the electron interacts with a field that varies in both space and time. This issue was first addressed in [23] where the Lewenstein model was extended by adding a linear term to the electric field. In our study, HHG from a nano-scale hot spot is simulated by a numerical solution of the time-dependent Schrödinger equation (TDSE), which is modified to take into account the spatial dependence of the electric field in the hot spot. We implement the length gauge transformation $\Psi_L(\vec{r}, t) = \Psi(\vec{r}, t) \exp((ie/\hbar) \int_0^t \vec{A}(\vec{r}', t) d\vec{r}')$, where $\Psi(\vec{r}, t)$ is the electron wavefunction and $\vec{A}(\vec{r}, t)$ is the vector potential of the driving laser. In the dipole

approximation, $\vec{A}(\vec{r}, t) = \vec{A}(t)$ and so $\Psi_L(\vec{r}, t) = \Psi(\vec{r}, t) \exp(\frac{ie}{\hbar} \vec{A} \cdot \vec{r})$. The TDSE within the length gauge is given by

$$i\hbar \frac{d\Psi_L(\vec{r}, t)}{dt} = \left\{ -\frac{\hbar}{2m} \nabla^2 + e\varphi(\vec{r}, t) + V_a(\vec{r}) \right\} \Psi_L(\vec{r}, t), \quad (1)$$

where $V_a(\vec{r})$ is the atomic potential and $\varphi(\vec{r}, t)$ is the electric potential of the driving laser (electric field is $\vec{E}(\vec{r}, t) = -\vec{\nabla}\varphi(\vec{r}, t)$). The effects of the magnetic field are neglected in equation (1) because we assume a moderate intensity level of the driving laser, which cannot accelerate the electron to relativistic velocity. The electric field of the driving laser within the hot spot is approximately a standing wave because the size of the hot spot (several nanometers) is much smaller than the wavelength of the driving laser ($\lambda_0 = 0.8 \mu\text{m}$). Specifically, we assume the field $E(\vec{r}, t) = \xi_{\text{hs}}(\vec{r}) \cos[\omega_0 t + \phi_{\text{noise}}(t)]$, where $\xi_{\text{hs}}(\vec{r})$ is the field spatially-dependent amplitude, ω_0 is the optical frequency and phase noise $\phi_{\text{noise}}(t)$ is a stochastic function that describes the coherence of the pump. Furthermore, we use the two-dimensional (2D) model: $\xi_{\text{hs}}(\vec{r}) = \xi_{\text{hs}}(x, y)$, where the electric field is x -polarized and atoms move in the x - y -plane. The electron is accelerated by the laser to a velocity that is much larger than the thermal velocity of the atom that crosses the hot spot. Thus, the electron experiences an effective pulsed electric potential that is given by

$$\varphi(x, x_a, y_a, t) = -\cos[\omega_0 t + \phi_{\text{noise}}(t)] \int_{x_a}^x \xi_{\text{hs}}(x', y_a) dx', \quad (2)$$

where $x_a = x_{0a} + v_x t$, $y_a = y_{0a} + v_y t$ are the coordinates of the atom that moves through the hot spot with velocity (v_x, v_y) . Neglecting the transverse broadening of the electron wave-packet, the TDSE is simplified to

$$i\hbar \frac{d\Psi_L(x, t)}{dt} = \left\{ -\frac{\hbar}{2m} \frac{\partial^2}{\partial x^2} + V_a(x) + e\varphi(x, x_a, y_a, t) \right\} \Psi_L(x, t). \quad (3)$$

The atomic potential of xenon was approximated by an inverse Gaussian potential [25]: $V_a(x) = -V_0 \exp[-(x/x_0)^2]$ with $V_0 = 17 \text{ eV}$ and $x_0 = 0.14 \text{ nm}$ (ionization potential $I_p = 12 \text{ eV}$). For simplicity, we assume a cylindrically symmetric Gaussian hot spot: $\xi_{\text{hs}}(x, y) = \xi_{0\text{hs}} \exp\{-(x^2 + y^2)/w_{\text{hs}}^2\}$ with hot spot width $w_{\text{hs}} = 0.6 \text{ nm}$ and peak amplitude $\xi_{0\text{hs}} = 1.23 \times 10^{10} \text{ V m}^{-1}$, which corresponds to peak intensity $I_0 = 2 \times 10^{13} \text{ W cm}^{-2}$.

The HHG field radiated by an atom with initial coordinates $(x_{0a}$ and $y_{0a})$ and velocities $(v_x$ and $v_y)$, $E_{\text{HHG}}^S(t, x_{0a}, y_{0a}, v_x, v_y)$, is calculated by the acceleration expectation value, using the Ehrenfest theorem $E_{\text{HHG}}^S(t, x_{0a}, y_{0a}, v_x, v_y) \propto \langle \Psi_L(x, t) | dV_a(x)/dx | \Psi_L(x, t) \rangle$.

Importantly, the dimension of the hot spot is much smaller than the wavelengths of the HHG radiation. Hence, we consider the hot spot as a point-source, neglecting its spatial dependence.

In section 3, we solve equation (3) and calculate the emitted field for a single atom that crosses the hot spot. In section 4, HHG emission from multiple atoms crossing the hot spot is calculated. For multiple atoms, equation (3) is solved N times ($m = 1, 2, 3, \dots, N$ atoms crossing the hot spot). We have simulated two cases. In the first case, the hot spot resides in a thermal gas of atoms so that the velocities $(v_x^m$ and $v_y^m)$ are random variables that are distributed according to the Maxwell-Boltzmann statistics. In the second case, the hot spot resides in a gas-jet or moves through the thermal gas with a velocity that is much higher than the gas thermal velocity. Atom velocities in this case correspond to the gas-jet (hot spot) velocity. In both cases,

the initial atom coordinates (x_{0a}^m and y_{0a}^m) are random variables that are distributed uniformly and the total radiated HHG field is calculated by a coherent super position of the partial fields.

As will be shown below, the important parameter that determines the line shape and bandwidth of the harmonics is the ratio between the coherence time of the pump laser (t_c)—the time interval over which $\phi_{\text{noise}}(t)$ is, on average, predictable—and the characteristic time interval in which the atoms cross through the hot spot. This cross-duration is given by $\tau = w_{\text{hs}}/\langle|\bar{v}|\rangle$ where $\langle|\bar{v}|\rangle$ is the average velocity of the atoms. In this work, we are interested in the highly coherent regime: $t_c \ll \tau$. For $\langle|\bar{v}|\rangle = 137 \text{ m s}^{-1}$ ($\tau = 4.4 \text{ ps}$ and $t_c = 2.6 \text{ ns}$), which is the characteristic thermal velocity of xenon at STP condition, the required computation time and memory is beyond our access. In order to relax this technical difficulty, we carried out the numerical simulations assuming the following parameters: $\langle|\bar{v}|\rangle = 2 \times 10^3 \text{ m s}^{-1}$ ($\tau = 0.3 \text{ ps}$ and $t_c = 180 \text{ ps}$), maintaining the highly coherent pump regime.

3. Single-atom spectra

We first present HHG spectra of a single atom that crosses the hot spot at a constant velocity of $v = 2 \times 10^3 \text{ m s}^{-1}$ for several trajectories (figures 1(a) and (b)). In these calculations, the phase noise did not affect the spectra because the coherence time was much longer than the cross-duration. All the trajectories are straight lines (deviation due to the pondermotive force is tiny [26]) and are characterized by their orientation with respect to the hot-spot polarization and their distance of closest approach to the center of the hot spot, which we designate with D . Figures 1(a) and (b) show the HHG spectra of atoms that cross the hot spot with velocity perpendicular (y -trajectory) and parallel (x -trajectory) to the field polarization, respectively, by atoms with through- and off-center trajectories. As shown, both odd and even harmonics are emitted. Even harmonics are emitted due to the nano-scale of the hot spot, which results in asymmetry between the right and left electron boomerang loops. The right–left symmetry is maintained and odd harmonics are absent for the through-center y -trajectories (figure 1(a)). Figure 1(c) shows a nontrivial dependence of the amplitude and phase of the $q = 11$ harmonic order (the cut-off harmonic) with respect to the distance of closest approach. Interestingly, trajectories passing through the center of the hot spot are not the most efficient ones. In fact, the amplitude peak in figure 1(c) at $D \sim 0.2 \text{ nm}$ corresponds to the situation in which the turning point of the traveling electron (point R in figure 1(d)) coincides with the center of the hot spot. As shown in figure 1(c), the intrinsic phase also exhibits a nontrivial dependence, which is not proportional to the peak intensity experienced by the atom, as in the case when the field is homogeneous [27]. Figures 1(e) and (f) show the emitted electric field of the $q = 11$ harmonic order by atoms with y - and x -trajectories, respectively. The parallel trajectory emits a two-peak pulse because it includes two ‘most efficient’ points (points R and L in figure 1(g)).

Next, we derive an analytical model for the harmonic line shape that is emitted by a single atom that crosses the hot spot at a perpendicular (y) trajectory (the model will be extended to multiple atoms in section 3). An atom that crosses our Gaussian-shaped hot spot ($\xi_{\text{hs}}(x, y) = \xi_{0\text{hs}} \exp[-(x^2 + y^2)/w_{\text{hs}}^2]$) at velocity v_y experiences an effective Gaussian driving pulse $G(t) = \exp(-t^2/\tau^2)$ with pulse-width (the atom cross-duration) $\tau = w_{\text{hs}}/v_y$. We invoke a simple model: the field of the q th-order harmonic is given by a product between the p th power of the effective driving pulse [28] and a complex amplitude, A_D , that depends on D according to figure 1(c):

$$E_q^S(t, D) = A_D [G(t)]^p \exp[iq(-\omega_0 t + \phi_{\text{noise}}(t))] + \text{c.c.} \quad (4)$$

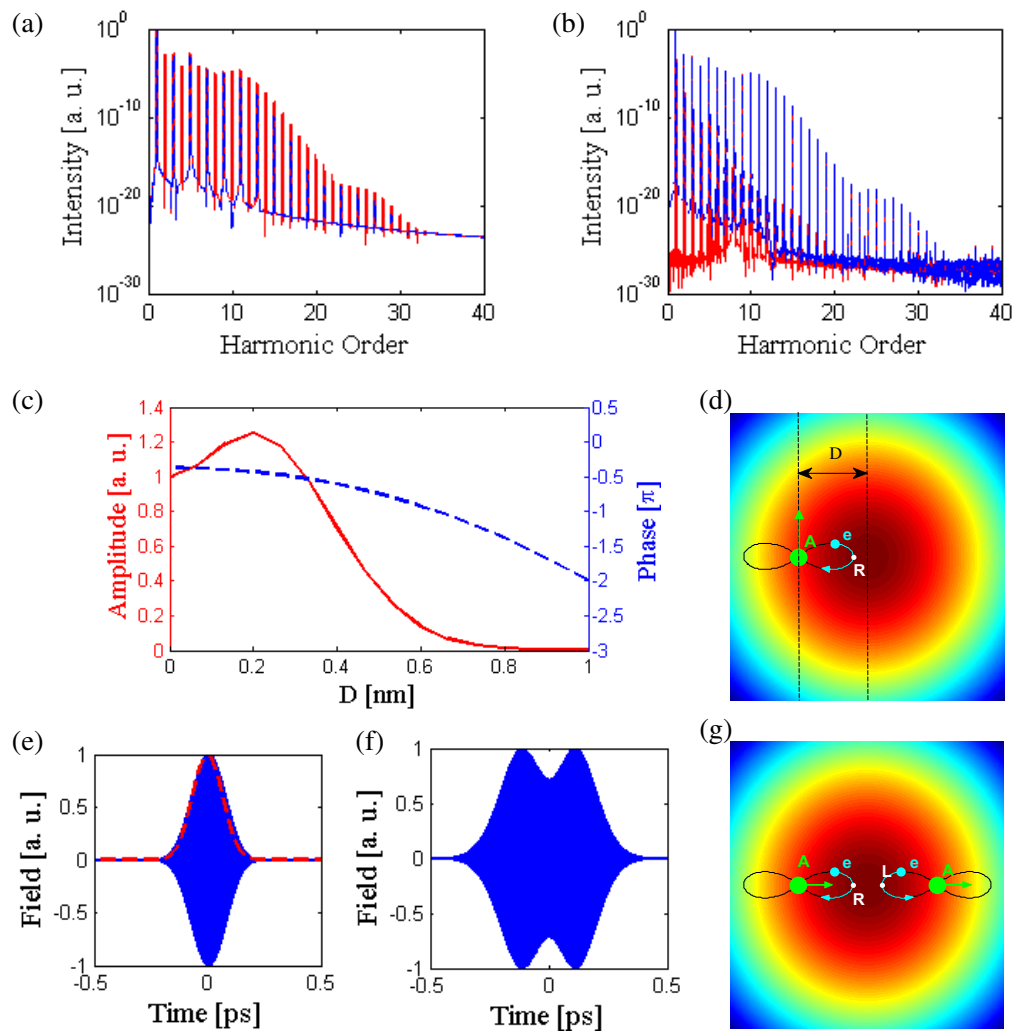


Figure 1. High-order harmonics by a xenon atom that crosses the hot spot at $v = 2 \times 10^3 \text{ m s}^{-1}$. The width and peak intensity of the hot spot are $w_{\text{hs}} = 0.6 \text{ nm}$ and $I_0 = 2 \times 10^{13} \text{ W cm}^{-2}$, respectively. Spectra emitted by an atom that crosses the hot spot with velocity perpendicular (a) and parallel (b) to the polarization of the hot spot at trajectories that cross through (blue-dashed line) and off (red-solid line) the center of the hot spot. In plots (c)–(e), the atom cross the hot spot perpendicular to its polarization. (c) Amplitudes (red-solid line) and phase (blue-dashed line) of the $q = 11$ harmonic-order (the cut-off harmonic) versus the distance of the closest approach of the atom to the hot-spot center (D). (d) Schematic representation of the off-center atom trajectory and electron oscillations when the atom crosses the hot spot perpendicular to the hot-spot polarization. Point R marks the point at which the distance between the boomeranging electron and atom is largest. (e), (f) Emitted electric field of the 11th-order harmonic by the atom that crosses the hot spot perpendicular to (e) and parallel (f) to its polarization. The red-dashed curve in (e) corresponds to $[G(t)]^{11}$ in equation (4). (g) Schematic representation of the through-center atom trajectory and electron oscillations when the atom crosses the hot spot parallel to its polarization.

The pulse-width of the q th-order harmonic field is $\tau' = w_{\text{hs}}/\sqrt{p}v_y$. We found that $q = 11$, $p = 11$ give the best fit to the numerical results (figure 1(e)). The energy spectral line shape of the q th-order harmonic is given by the ensemble average over the Fourier transform of the autocorrelation function:

$$\left\langle \left| \tilde{E}_q^S(\omega) \right|^2 \right\rangle = \left\langle \mathcal{F} \left\{ \int dt' E_q^S(t') E_q^{S*}(t+t') \right\} \right\rangle. \quad (5)$$

Substituting equation (4) into (5) and averaging out the terms oscillating at twice the optical frequency leads to

$$\left\langle \left| \tilde{E}_q^S(\omega) \right|^2 \right\rangle = \frac{1}{2} |A_D|^2 \left[\left| \tilde{G}^p(\omega - q\omega_0) \right|^2 \otimes \tilde{L}(\omega) + \left| \tilde{G}^p(\omega + q\omega_0) \right|^2 \otimes \tilde{L}(\omega) \right]. \quad (6)$$

In equation (6), \otimes stands for convolution, $|\tilde{G}^p(\omega)|^2 = \mathcal{F}[\int dt' G^p(t') G^p(t+t')] = \pi \tau'^2 \exp(-\omega^2 \tau'^2/2)$ and the Lorentzian $\tilde{L}(\omega) = \mathcal{F}\{(\exp[iq \Delta \phi_{\text{noise}}(t)])\} = 2q^2 \delta\omega_{\text{pump}}/(\omega^2 + q^2 \delta\omega_{\text{pump}})$, where $\Delta \phi_{\text{noise}}(t) = \phi_{\text{noise}}(t+t') - \phi_{\text{noise}}(t')$ and $\delta\omega_{\text{pump}}$ is the spectral bandwidth of the pump. The Lorentzian term is associated with the phase noise of the pump. Note that for $q = 1$, the Lorentzian corresponds to the spectrum of the pump with spectral bandwidth $\delta\omega_{\text{pump}}$, which results from the phase noise [29].

The convolution in equation (6) can be expressed in terms of the Faddeeva function, which is well known in plasma physics [30]. Thus, the energy spectrum can be expressed by

$$\left\langle \left| \tilde{E}_q^S(\omega) \right|^2 \right\rangle = \pi \tau'^2 |A_D|^2 \text{Re} \left\{ W \left[\tau' (\omega - q\omega_0 + iq^2 \delta\omega_{\text{pump}})/\sqrt{2} \right] + W \left[\tau' (\omega + q\omega_0 + iq^2 \delta\omega_{\text{pump}})/\sqrt{2} \right] \right\}, \quad (7)$$

where the Faddeeva function is given by $W(y) = \exp(-y^2) \text{erfc}(-iy)$. In the limiting case of a highly coherent pump, $q^2 \delta\omega_{\text{pump}} \tau' \ll 1$, the real part of the Faddeeva function is well approximated by a Gaussian $\text{Re} \left\{ W \left[\tau' (\omega + iq^2 \delta\omega_{\text{pump}})/\sqrt{2} \right] \right\} \approx \exp(-\omega^2 \tau'^2/2)$; hence, the energy spectrum is given by

$$\left\langle \left| \tilde{E}_q^S(\omega) \right|^2 \right\rangle \approx \pi \tau'^2 |A_D|^2 \left\{ \exp[-\tau'^2 (\omega - q\omega_0)^2/2] + \exp[-\tau'^2 (\omega + q\omega_0)^2/2] \right\}, \quad (8)$$

and its bandwidth is inversely proportional to the pulse width of the harmonic field $\Delta\omega_q \approx 1/\tau'$. In the opposite limiting case of the low-coherence pump, $q^2 \delta\omega_{\text{pump}} \tau' \gg 1$, the real part of the Faddeeva function is well approximated by a Lorentzian: $\text{Re} \left\{ W \left[\tau' (\omega + iq^2 \delta\omega_{\text{pump}})/\sqrt{2} \right] \right\} \approx \sqrt{2} q^2 \delta\omega_{\text{pump}} / [\sqrt{\pi} \tau' (q^4 \delta\omega_{\text{pump}}^2 + \omega^2)]$ and the energy spectrum is given by

$$\left\langle \left| \tilde{E}_q^S(\omega) \right|^2 \right\rangle \approx \sqrt{\frac{\pi}{2}} \tau' q^2 \delta\omega_{\text{pump}} |A_D|^2 \left\{ \frac{1}{[q^4 \delta\omega_{\text{pump}}^2 + (\omega - q\omega_0)^2]} + \frac{1}{[q^4 \delta\omega_{\text{pump}}^2 + (\omega + q\omega_0)^2]} \right\}, \quad (9)$$

and its bandwidth is given by $\Delta\omega_q \approx q^2 \delta\omega_{\text{pump}}$. Thus, in the case of a high-coherent pump, the spectral line shape is determined by the structure of the hot spot. In our example, the Gaussian line shape corresponds to the Fourier transform of the Gaussian hot spot. In the case of a low-coherence pump, the spectral line shape is defined by the spectral line shape of the pump, which is typically a Lorentzian.

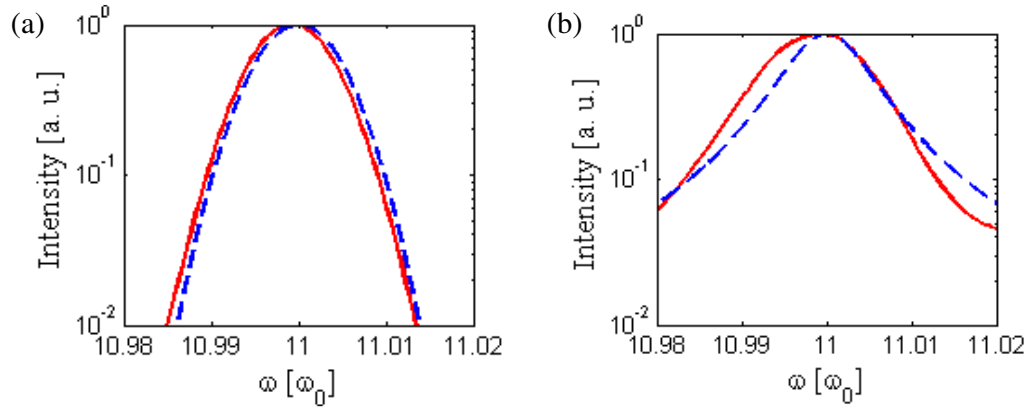


Figure 2. Energy spectra of 11th-order harmonic with high (a) and low (b) coherent pumps. Red-solid lines correspond to the numerical solution of equation (3). Blue-dashed lines correspond to the analytical model: equation (8) in panel (a) and equation (9) in panel (b). Deviation between the analytical and numerical curves is due to a resonant absorption of the pump at 12 eV (see figure 1(a)).

Comparison between the analytical model and numerical solution of equation (3) is shown in figure 2. Figure 2(a) shows the 11th-order harmonic for the case of highly coherent pump ($\delta\omega_{\text{pump}}/\omega_0 = 2.4 \times 10^{-6}$ and $v_y = 2 \times 10^3 \text{ m s}^{-1}$ result with $q^2\delta\omega_{\text{pump}}\tau' = 6 \times 10^{-2}$). As shown, the numerically calculated spectral line shape (solid line) matches quite well to a Gaussian given by equation (8) (dashed line). Figure 2(b) shows the 11th-order harmonic in the opposite case of low-coherence pump ($\delta\omega_{\text{pump}}/\omega_0 = 4.4 \times 10^{-5}$ and $v_y = 10^3 \text{ m s}^{-1}$ result in $q^2\delta\omega_{\text{pump}}\tau' = 2.4$). In this case, the spectral line shape is determined by the bandwidth of the pump and it is approximated by the Lorentzian in equation (9).

4. Multiple atoms spectra

In the previous section, we presented the numerical and analytical results of single-atom harmonic spectra. We showed that when the coherence time of the pump laser is much larger than the atom cross-duration then the harmonics bandwidth is inversely proportional to the cross-duration and does not depend on the coherence of the pump. In this section, we investigate the emission from multiple atoms that cross the hot spot with random trajectories, velocities and times. One may expect the randomness to reduce the coherence of the harmonics and, equivalently, increase their spectral bandwidth. Below, we show that the harmonics line shapes actually include a narrow spike that reflects the high coherence of the pump laser.

The emitted spectral line shapes from a thermal gas (red-solid line) and from a gas jet (blue-dashed line) are shown in figures 3(a) and (b) for the case of a highly coherent pump ($\delta\omega_{\text{pump}}/\omega_0 = 2.4 \times 10^{-6}$ and $v_y = 2 \times 10^3 \text{ m s}^{-1}$ result in $q^2\delta\omega_{\text{pump}}\tau' = 6 \times 10^{-2}$). The 2D density of atoms was $n_V = 10^{19} \text{ cm}^{-3}$ and hot spot height was $H_{\text{hs}} = 50 \text{ nm}$. The rest of the simulation parameters are listed in section 2. One can see in figure 3(b) that the spectral line shape comprises a wide bell-shaped curve and narrow spike on top of it. As will be shown below, the wide bell-shaped curve is associated with the single-atom emission, which was

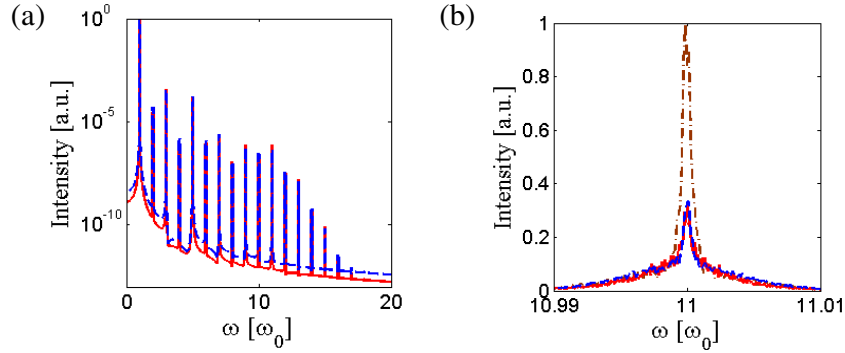


Figure 3. Numerical emission spectra from three stochastic processes: thermal gas (red-solid line), gas-jet (blue-dashed line) and an artificial case in which all the atoms cross the hot spot through the same trajectory (brown dashed-dot line). Full spectrum is shown in panel (a) and the zoomed region around the 11th harmonic is shown in panel (b).

analyzed in the previous section, while the narrow spike results from collective emission of atoms.

Below, we derive an analytical expression for the spectral line shape for an artificial case in which all the atoms cross the hot spot through the same trajectory. In this case, the times at which the atoms cross the hot spot remain the only stochastic variables. Numerically calculated line shape for this artificial case is also plotted in figure 3(b) (brown dashed-dot line). Clearly, all cases exhibit a qualitatively similar shape: a narrow spike on top of a wide bell-shaped curve (the difference in amplitudes is explained below).

Next, we introduce an analytical model for the spectral line shape of collective emission. Since both the thermal gas and the gas-jet cases exhibit a similar spectral line shape, we limit our model to the simpler gas-jet case by assuming that all atoms have perpendicular (y) trajectories and equal velocities v_y . The averaged flux of atoms F crossing the hot spot with velocity v_y is given by $F = n_v v_y$. The collective field emitted by N atoms that (stochastically) cross the hot spot can be represented as a super-position of fields emitted by individual atoms:

$$E_q^C(t) = \sum_{n=1}^N E_q^S(t - t_0^n, D_n), \quad (10)$$

where E_q^S is the single-atom field given by equation (4), and time and distance of the closest approach are given by $t_0^n = (y_{\text{center}} - y_0^n)/v_y$ and $D_n = x_0^n$, respectively. Both time and distance of the closest approach are random variables because of the random initial coordinates of atoms (x_0^n and y_0^n), which are stochastically distributed in space. The sequence of N pulses represented by equation (10) can be modeled as a linearly filtered Poisson process [31]. The power spectral density of such a sequence is represented by [31]

$$S(\omega) = \lim_{X \rightarrow \infty} \lim_{T \rightarrow \infty} \frac{1}{T} \left[\frac{\langle N \rangle}{TX} \int_{-X/2}^{X/2} dD \int_{-T/2}^{T/2} dt_0 \left| \int_{-T/2}^{T/2} dt \exp(i\omega t) E_q^S(t - t_0, D) \right|^2 + \frac{\langle N^2 - N \rangle}{T^2 X^2} \left| \int_{-X/2}^{X/2} dD \int_{-T/2}^{T/2} dt_0 \int_{-T/2}^{T/2} dt \exp(i\omega t) E_q^S(t - t_0, D) \right|^2 \right], \quad (11)$$

where $\langle N \rangle$ is the average number of atoms crossing the hot spot $\langle N \rangle / (TX) = FH_{\text{hs}}$ and $\langle N^2 - N \rangle (TX)^2 = F^2 H_{\text{hs}}^2$. The first term on the rhs of equation (11) can be associated with the spectral line shape of single-atom emission, and can be expressed in terms of the Faddeeva function (see equation (7)). The second term, resulting from the collective emission of atoms, can be evaluated by substituting equation (4) for E_q^S . Using the convolution theorem and averaging out the terms oscillating at twice the optical frequency one finds that

$$S(\omega) = \sum_{\omega'=q\omega_0, -q\omega_0} \pi \tau'^2 FH_{\text{hs}} \left[\int_{-\infty}^{\infty} dD |A_D|^2 \text{Re} \left\{ \text{W} \left[\tau' (\omega - \omega' + iq^2 \delta\omega_{\text{pump}}) / \sqrt{2} \right] \right\} \right. \\ \left. + 2FH_{\text{hs}} \left| \int_{-\infty}^{\infty} dD A_D \right|^2 \frac{q^2 \delta\omega_{\text{pump}}}{(\omega - \omega')^2 + q^4 \delta\omega_{\text{pump}}^2} \right]. \quad (12)$$

Due to the nontrivial dependence of the complex amplitude, A_D , on D (figure 1(c)) we calculated the analytical spectra only for the artificial case in which all the atoms have a fixed trajectory (fixed D). The atom crossing rate of the hot spot was $2FH_{\text{hs}}L_{\text{hs}}$, where $L_{\text{hs}} = 2w_{\text{hs}}\sqrt{\lg(2)}$ is the hot spot full-width at half-maximum (atoms that cross the hot spot at $|D| > L_{\text{hs}}$ do not emit HHG due to the relatively low pump intensity). Equation (12) in this case reduces to

$$S(\omega) = \sum_{\omega'=q\omega_0, -q\omega_0} \pi \tau'^2 2FH_{\text{hs}}L_{\text{hs}} |A_D|^2 \left[\text{Re} \left\{ \text{W} \left[\frac{\tau' (\omega - \omega' + iq^2 \delta\omega_{\text{pump}})}{\sqrt{2}} \right] \right\} \right] \\ + 4FH_{\text{hs}}L_{\text{hs}} \frac{q^2 \delta\omega_{\text{pump}}}{(\omega - \omega')^2 + q^4 \delta\omega_{\text{pump}}^2}. \quad (13)$$

The analytical spectral line shapes (equation (13)) are shown in figures 4(a)–(c) (red-dashed curves) at different coherence and flux conditions. Figures 4(a) and (b) show the spectral line shape of 11th-order harmonic for highly coherent pump ($q^2 \delta\omega_{\text{pump}} \tau' = 6 \times 10^{-2}$) in the case of high $FH_{\text{hs}}w_{\text{hs}}/\delta\omega_{\text{pump}} = 85$ and low $FH_{\text{hs}}w_{\text{hs}}/(\delta\omega_{\text{pump}}) = 4.85$ fluxes, respectively. The spectral line shapes comprise a wide bell-shaped curve and a narrow spike on top of it. The wide bell-shaped curve associated with the single-atom emission is given by the Faddeeva function (the first term on the rhs in equation (13)). It is well approximated by a Gaussian with its bandwidth defined by the inverse of the cross-duration $\Delta\omega_1 \sim v_y \sqrt{p}/w_{\text{hs}}$. The narrow spike is given by the second term in equation (13), which results from phase-locked emission from the collective atoms. The line shape of this spike is Lorentzian with $\Delta\omega_2 \sim q^2 \delta\omega_{\text{pump}}$ bandwidth. The amplitude of the narrow spike is proportional to the atomic flux (note the different amplitudes in figures 4(a) and (b).) Intuition for the narrow spike (high coherence) is provided from figures 4(d) and (e) that show the corresponding emitted fields schematically. As shown, the fields consist of a highly coherent carrier wave (locked with the pump) and stochastic envelopes (atoms cross the hot spot at random times). The narrow spike is associated with the coherent carrier wave and it is large when the flux is high (figures 4(a) and (c)).

Spectral line shape and the corresponding schematic field for the low-coherence pump case ($q^2 \delta\omega_{\text{pump}} \tau' = 2.4$) are shown in figures 4(c) and (f), respectively. In this case, the first and second terms in equation (13) are approximated, respectively, and given by the same Lorentzian ($\Delta\omega \sim q^2 \delta\omega_{\text{pump}}$). The spectral line shape in this case does not include a narrow spike and correspondingly, the carrier wave does not maintain coherence for periods larger than the cross-duration. Finally, corresponding numerical line shapes (obtained by solutions of TDSE for the

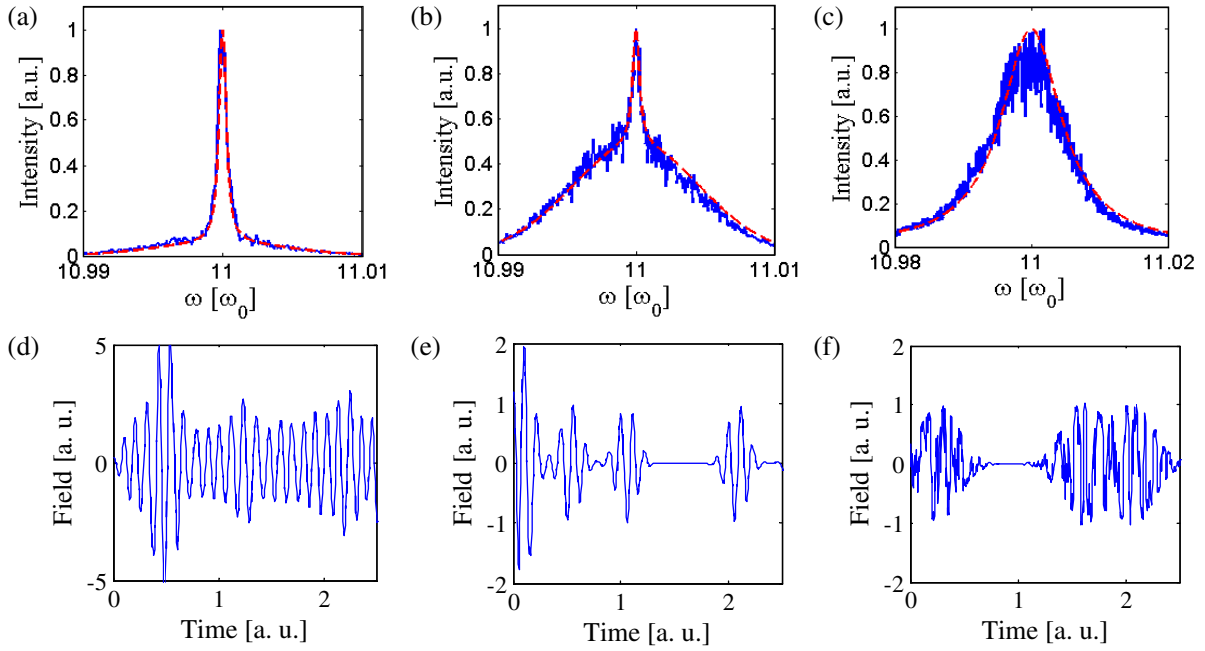


Figure 4. Spectral line shapes in the high-coherence regime for high (a) and low (b) flux of atoms, and in the low-coherence regime (c). Dashed red lines represent the analytical results (equation (13)) and solid blue lines represent numerical results (also for the artificial case). Schematic representation of the emitted fields in the high-coherence regime for high (d) and low (e) flux of atoms, and in the low-coherence regime (f).

artificial case) are also plotted in figures 4(a)–(c) (blue-solid curves), showing good agreement between numerical and analytical results.

Now that we understand the spectral properties of the emission in the artificial case (all atoms cross the hot spot with the fixed trajectory), we return to the case of random trajectories (thermal gas or gas jet). Numerically calculated spectra of thermal and gas-jet cases are shown in figure 3. Figure 3(b) (brown curve) also shows the numerically calculated spectral line shape in the artificial case. Clearly, the spectral lines of the three cases exhibit the narrow spike on top of the broad Gaussian, yet the amplitudes of the real cases are reduced. According to equation (12) (gas jet) and equation (13) (artificial case), the ratios between the widths of the narrow spike and Gaussian are approximately given by $2FH_{\text{hs}}|\int_{-L_{\text{hs}}}^{L_{\text{hs}}} dDA_D|^2/\int_{-L_{\text{hs}}}^{L_{\text{hs}}} dD|A_D|^2$ and $4FH_{\text{hs}}L_{\text{hs}}$, respectively. The reduction in the spike amplitude is due to the fact that $|\int_{-L_{\text{hs}}}^{L_{\text{hs}}} dDA_D|^2 < 2L_{\text{hs}}\int_{-L_{\text{hs}}}^{L_{\text{hs}}} dD|A_D|^2$ when the phase of A_D is not a constant. That is, the reduction results from the fact that the intrinsic (and total) phase in HHG depends on the pump peak intensity, which in the hot spot geometry is determined by the distance of closest approach—a stochastic variable. The narrow spike disappears when the hot spot intensity and geometry results with $|\int_{-\infty}^{\infty} dDA_D|^2 \approx 0$. Going back to figure 1(c), one can see that in our hot spot and pump intensity, the phase of A_D varies in the range of $\pi/2$ within the range in which the HHG emission is strong. This observation explains the existence of the narrow spikes (figure 3(b)), even though the emission process results from multiple atoms that cross the hot spot at random trajectories and random times.

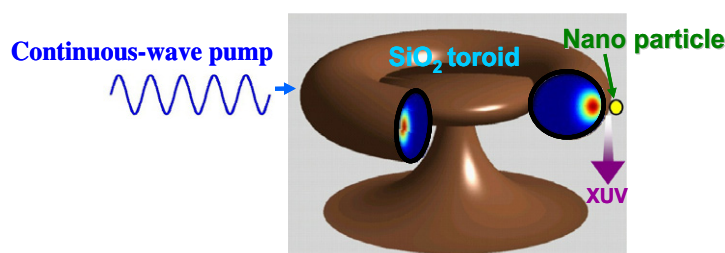


Figure 5. Schematic representation of the on-chip device for the continuous-wave generation of high-order harmonics. The driving laser circulates azimuthally in a silica whispering-gallery micro-resonator. The cut shows the electric field in a plane transverse to (azimuthal) propagation, which extends beyond the silica into the surrounding gas. A nano-antenna (e.g. gold nano-sphere) enhances the field at the gap between the nano-particle and the micro-resonator. High-order harmonics are emitted by the atoms that cross the localized strong laser hot spot.

5. Generation of high-intensity long-duration hot spots

In the previous sections, we investigated spectral properties of high-order harmonics emitted by atoms that cross long-duration nanometer-scale hot spots, which are intense enough to generate high harmonics. In this section, we present qualitatively a scheme that produces such a long-duration highly coherent hot spot. The proposed device cascades two enhancement mechanisms: enhancement by multiple recirculation within high-quality micro-resonator and further enhancement by focusing with a nano-antenna. A representative device is shown in figure 5, showing a metallic nano-particle (e.g. gold nano-sphere or bow-tie nano-antennas [11, 12]) that is located outside, yet in very close proximity, to the surface of a silica ultrahigh-quality toroidal whispering-gallery micro-resonator [16–18], similarly ultrahigh-quality crystalline resonators can be used [19–21].

The modes propagating in the whispering-gallery micro-resonator extend evanescently beyond the silica into the near-field in the surrounding region. Metallic nano-particles can interact with this evanescent field and focus the extended part of the mode into sub-wavelength hot spots, thereby enhancing its intensity by orders of magnitude (with theoretical enhancement factor of $\sim 10^2$ – 10^3 [22]). Taking advantage of the accumulated field enhancements from the multiple re-circulations in the micro-resonator, which exhibit a finesse of $\sim 10^6$, and from the nano-scale plasmonic enhancement [32, 33], the intensity threshold for HHG may be achieved. These nano-scale hot spots are located in the gaps between the micro-cavity and the nano-structures. An atom that crosses the nano-scale hot spot experiences a field of varying intensity in a similar fashion to an atom that is irradiated by a micro-scale picosecond pulse (the width of this ‘pulse’ can be controlled by the size of the hot spot and the characteristic velocity of the atoms, which is determined by the pressure and temperature of the gas). Hence, as explained in section 2, each atom is expected to emit high-order harmonics of the driving laser, despite the continuous nature of the driving force. While the instantaneous field that is emitted from this device is very small (due to the small size of the hot spots), the average emitted power can be comparable to the average power in other HHG-based schemes because emission from the proposed device is not limited to ultra-short bursts at relatively low repetition rate. Also, as

shown in section 3, this device can emit ultrahigh coherent EUV radiation, reflecting the fact that the driving laser light is circulating in a very high-quality micro-resonator. Even though atoms cross the hot spot at random times and trajectories (thermal gas), their HHG emission is highly phase correlated.

6. Conclusions

We have proposed and investigated a scheme for generating narrow bandwidth radiation in the EUV. The device that we propose is based on emission of high-order harmonics by atoms crossing the hot spot. The hot spot is produced by nano-antenna adjacent to high-quality toroidal micro-resonator. Our spectral analysis shows that for a high flux of atoms through the hot spot, the emission spectrum will be dominated by a narrow spike. The bandwidth of this narrow spike is determined by the bandwidth of the pump light. Such an ultra-narrow band radiation in EUV may enhance resolution in a wide range of applications including spectroscopy [34], precision measurements, coherent imaging [35], holography [36, 37], etc.

Acknowledgments

This work was supported by the Legacy Heritage fund of the Israel Science Foundation (ISF), the Marie Curie International Reintegration Grant (IRG) and USA–Israel Binational Science Foundation (BSF).

References

- [1] Attwood D T 1999 *Soft X-Rays and Extreme Ultraviolet Radiation: Principles and Applications* (Cambridge: Cambridge University Press)
- [2] McPherson A, Gibson G, Jara H, Johann U, Luk T S, McIntyre I A, Boyer K and Rhodes C K 1987 Studies of multiphoton production of vacuum-ultraviolet radiation in the rare gases *J. Opt. Soc. Am. B* **4** 595–601
- [3] Ferray M, L'Huillier A, Li X F, Lompré L A, Mainfray G and Manus C 1988 Multiple-harmonic conversion of 1064 nm radiation in rare gases *J. Phys. B: At. Opt. Phys.* **21** L31
- [4] Yost D, Schibli T, Ye J, Tate J, Hostetter J, Gaarde M and Schafer K 2009 Vacuum-ultraviolet frequency combs from below-threshold harmonics *Nature Phys.* **5** 815–20
- [5] Schafer K J and Kulander K C 1997 High harmonic generation from ultrafast pump lasers *Phys. Rev. Lett.* **78** 638–41
- [6] Barkauskas M, Brandi F, Giammanco F, Neshev D, Pirri A and Ubachs W 2005 A novel-type tunable and narrowband extreme ultraviolet radiation source based on high-harmonic conversion of picosecond laser pulses *J. Electron Spectrosc. Relat. Phenom.* **144–147** 1151–5
- [7] Corkum P B 1993 Plasma perspective on strong field multiphoton ionization *Phys. Rev. Lett.* **71** 1994–7
- [8] Hädrich S, Rothhardt J, Krebs M, Tavella F, Willner A, Limpert J and Tünnermann A 2010 High harmonic generation by novel fiber amplifier based sources *Opt. Express* **18** 20242–50
- [9] Gohle C, Udem T, Herrmann M, Rauschenberger J, Holzwarth R, Schuessler H A, Krausz F and Hansch T W 2005 A frequency comb in the extreme ultraviolet *Nature* **436** 234–7
- [10] Jones R J, Moll K D, Thorpe M J and Ye J 2005 Phase-coherent frequency combs in the vacuum ultraviolet via high-harmonic generation inside a femtosecond enhancement cavity *Phys. Rev. Lett.* **94** 193201
- [11] Boardman A D 1982 *Electromagnetic Surface Modes* (Chichester: Wiley)
- [12] Barnes W L, Dereux A and Ebbesen T W 2003 Surface plasmon subwavelength optics *Nature* **424** 824–30

- [13] Kim S, Jin J, Kim Y J, Park I Y, Kim Y and Kim S W 2008 High-harmonic generation by resonant plasmon field enhancement *Nature* **453** 757–60
- [14] Stockman M I 2008 An easier route to high harmony *Nature* **453** 731–3
- [15] Park I Y, Kim S, Choi J, Lee D H, Kim Y J, Kling M F, Stockman M I and Kim S W 2011 Plasmonic generation of ultrashort extreme-ultraviolet light pulses *Nature Photonics* **5** 677–81
- [16] Armani D K, Kippenberg T J, Spillane S M and Vahala K J 2003 Ultra-high- Q toroid microcavity on a chip *Nature* **421** 925–8
- [17] Spillane S M, Kippenberg T J, Painter O J and Vahala K J 2003 Ideality in a fiber-taper-coupled microresonator system for application to cavity quantum electrodynamics *Phys. Rev. Lett.* **91** 043902
- [18] Carmon T and Vahala K J 2007 Visible continuous emission from a silica microphotonic device by third-harmonic generation *Nature Phys.* **3** 430–5
- [19] Moore J, Tomes M, Carmon T and Jarrahi M 2011 Continuous-wave ultraviolet emission through fourth-harmonic generation in a whispering-gallery resonator *Opt. Express* **18** 24139–46
- [20] Grudinin I S, Matsko A B, Savchenkov A A, Strekalov D, Ilchenko V S and Maleki L 2006 Ultra high Q crystalline microcavities *Opt. Commun.* **265** 33–8
- [21] Sprenger B, Schwefel H G L, Lu Z H, Svitlov S and Wang L J 2010 CaF₂ whispering-gallery-mode-resonator stabilized-narrow-linewidth laser *Opt. Lett.* **35** 2870–2
- [22] Stebbings S L, Süßmann F, Yang Y-Y, Scrinzi A, Durach M, Rusina A, Stockman M I and Kling M F 2011 Generation of isolated attosecond extreme ultraviolet pulses employing nanoplasmonic field enhancement: optimization of coupled ellipsoids *New J. Phys.* **13** 073010
- [23] Husakou A, Im S -J and Herrmann J 2011 Theory of plasmon-enhanced high-order harmonic generation in the vicinity of metal nanostructures in noble gases *Phys. Rev. A* **83** 043839
- [24] Ciappina M F, Biegert J, Quidant R and Lewenstein M 2012 High-order-harmonic generation from inhomogeneous fields *Phys. Rev. A* **85** 033828
- [25] Ben-Tal N, Moiseyev N and Kosloff R 1993 Harmonic generation in ionizing systems by the complex scaled adiabatic-switch method *Phys. Rev. A* **48** 2437–42
- [26] Eichmann U, Nubbemeyer T, Rottke H and Sandner W 2009 Acceleration of neutral atoms in strong short-pulse laser fields *Nature* **461** 1261–4
- [27] Lewenstein M, Salieres P and L’Huillier A 1995 Phase of the atomic polarization in high-order harmonic generation *Phys. Rev. A* **62** 4747–54
- [28] Peatross J, Voronov S and Prokopovich I 1997 Selective zoning of high harmonic emission using counter-propagating light *Opt. Express* **1** 114–25
- [29] Yariv A and Yeh P 2007 *Photonics: Optical Electronics in Modern Communication* (New York: Oxford University Press)
- [30] Fried B D and Conte S D 1961 *The Plasma Dispersion Function* (New York: Academic)
- [31] Goodman J W 2000 *Statistical Optics* (New York: Wiley Classics Library Edition)
- [32] Kaplan A E, Carmon T, Kozlov M, Cohen O, Bartal G and Schwefel H G L Intensity enhancement by microtoroid and metal nanosphere coupling in preparation
- [33] Xiao Y F, Liu Y C, Li B B, Chen Y L, Li Y and Gong Q 2012 Strongly enhanced light-matter interaction in a hybrid photonic-plasmonic resonator *Phys. Rev. A* **85** 031805
- [34] Cingöz A, Yost D C, Allison T K, Ruehl A, Fermann M E, Hartl I and Ye J 2012 Direct frequency comb spectroscopy in the extreme ultraviolet *Nature* **482** 68–71
- [35] Sandberg R L, Paul A P, Raymondson D, Hädrich S, Gaudiosi D, Holtsnider J, Tobey R, Cohen O, Murnane M M, Kapteyn H C, Song C, Miao J, Liu Y and Salmassi F 2007 Lensless diffractive imaging using tabletop coherent high harmonic soft x-ray beams *Phys. Rev. Lett.* **99** 098103
- [36] Tobey R I, Siemens M E, Cohen O, Murnane M M, Kapteyn H C and Nelson K A 2007 Ultrafast extreme ultraviolet holography: dynamic monitoring of surface deformation *Opt. Lett.* **32** 286–8
- [37] Bartels R A, Paul A, Green H, Kapteyn H C, Murnane M M, Backus S, Christov I P, Liu Y, Attwood D and Jacobsen C 2002 Generation of spatially coherent light at extreme ultraviolet wavelengths *Science* **297** 376–8